



Deformation microstructures and texture evolution of the Mg–Zn–Mn alloy with high strain rate rolling

Qin Wu¹, Caihe Fan^{1,3,a)}, Hongge Yan^{2,a)}, Jianjun Yang¹, Dongsheng Zheng¹, Ling Ou¹, Zeyi Hu¹, Yumeng Ni¹

¹School of Materials and Advanced-Manufacturing, Hunan University of Technology, Zhuzhou 412007, China

²School of Materials Science and Engineering, Hunan University, Changsha 410082, China

³Anhui Jianye Science and Technology Co., Ltd., Huaibei 235000, China

^{a)}Address all correspondence to these authors. e-mails: 369581813@qq.com; yanhg68@163.com

Received: 3 August 2022; accepted: 7 November 2022; published online: 29 November 2022

The effect of strain rates ($\dot{\epsilon}$) on the microstructure, texture, and mechanical properties of the Mg–5Zn–0.6Mn alloys during high strain rate rolling at 300 °C are studied. Increasing $\dot{\epsilon}$ promotes dynamic recrystallization (DRX). The DRX grain grows from 1.0 to 3.4 μm , and the DRX volume fraction increases from 76 to 93% with $\dot{\epsilon}$ rising from 10 to 25 s^{-1} . The maximum intensity values of basal texture decrease from 2.74 to 2.09 with increasing $\dot{\epsilon}$. The texture weakening is mainly attributed to the increase in DRX volume fraction and the number of tensile twins. The alloy sheets rolled at 10 s^{-1} possess optimal comprehensive mechanical properties (the tensile strength of 321 MPa, yield strength of 240 MPa, and elongation of 24.9%), attributing to the smallest DRX grain size, and the largest geometrically necessary dislocations density and precipitation density.

Introduction

The Mg–Zn alloys are easy to form a strong (0002) basal texture during rolling, which leads to anisotropic mechanical properties and increases the difficulty of secondary forming [1]. Therefore, texture modification is one of the critical ways to develop high strength and high plastic wrought Mg–Zn alloy sheets. The processing technology, deformation parameters, and alloying elements are the main factors affecting the texture characteristics of Mg alloys.

There are many reports about the influential mechanism of alloying elements on the texture characteristics in Mg alloys. Masoumi et al. [2] have found that the basal texture weakening in the as-deformed Mg–Zn–Sr alloys is mainly due to the particle excited nucleation (PSN) mechanism during dynamic recrystallization. However, some texture weakening phenomena cannot be explained clearly through the PSN mechanism. Even if there are large-sized phases existed in some Mg alloys, the texture weakening cannot be observed [3]. Stanford et al. [4] have proposed the shear band-induced nucleation (SBIN) mechanism to explain the formation of a new texture (i.e., $\langle 111 \rangle$ rare earth texture) in the as-extruded Mg–1.55Gd alloy.

The Mg alloy texture can be optimized by introducing appropriate shear deformation in the plastic forming process.

Kim et al. [5] have reported that the basal texture is significantly weakened in the AZ31 alloy as induced repeated shear deformation by combining the equal channel angular rolling and asynchronous rolling processes. Pan et al. [6] have found that the (0002) texture of the Mg–2Zn–2Gd alloy deviates about 40° along the normal direction after cross rolling.

The deformation parameters can also affect the texture characteristics. Chen et al. [7] have found that the DRX volume fraction increases with the increase of rolling temperature. The DRX volume fraction increase brings about more grains with random orientation, resulting in the basal texture weakening. Sanjari et al. [8] have found that the basal texture of Mg–Zn–xCe alloy plates splits along the rolling direction, and the maximum intensity values of basal texture in all alloys decrease with the rolling speed increases from 15 to 1000 m/min. Liu et al. [9] have found that the texture intensity of the Mg–4.5Zn–0.75Er (wt%) alloy increases first, then decreases, and then increases with the increase of strain at 200 °C, while it decreases with increasing the strain at 300 °C. Zheng et al. [10] have reported that the texture intensity of the Mg–5.25Zn–0.6Ca (wt%) alloy at extrusion temperatures of 270 °C, 300 °C, and 330 °C are 7.6, 6.8, and 7.7, respectively. Liu et al. [11] have also observed

that the texture intensity of the Mg–3Zn–1Ca–0.5Sr (wt%) alloy decreases first and then increases as hot compression from 300 to 390 °C. Comprehensive analysis of the existing literature, it is found that the influence of deforming technique parameters on texture characteristics is still controversial, and the main factors affecting texture and the correlation between texture and mechanical properties are still unclear.

Our previous study [12] has found that high strain rate rolling (HSRR) can significantly weaken the basal texture intensity of the alloy sheets compared with traditional rolling, but the main factors affecting the formation of texture, as well as the effect of texture on the mechanical properties of the as-HSRRed alloy sheets have not been deeply studied. Given this, the Mg–5Zn–0.6Mn alloys are subjected to HSRR with the rolling temperature of 300 °C and strain rates of 10 s⁻¹, 15 s⁻¹, 20 s⁻¹, and 25 s⁻¹ in this paper, the influence regularity and mechanism of rolling parameters on deformation microstructure characteristics (dislocation, twinning, dynamic recrystallization, and precipitation) and texture, as well as the effect of texture on mechanical properties are studied, to provide the experimental evidence and scientific bases for the development of texture modification technology.

Result

The as-rolled microstructures

Figure 1 illustrates the optical microscope (OM) images of the Mg–5Zn–0.6Mn alloy sheets HSRRed with different strain rates ($\dot{\epsilon}$) at 300 °C (transverse direction–rolling direction, TD–RD). It can be seen from Fig. 1(a) that DRX occurs in the alloy, and a small number of twins exist in the un-DRXed region at $\dot{\epsilon}$ of 10 s⁻¹. HSRR could induce strong twin activity [13], high-density twins divide the original coarse grains into smaller parts, and the high-density dislocations in the twins can accelerate the DRX process [14]. When $\dot{\epsilon}$ increases to 15 s⁻¹ [Fig. 1(b)], the DRX grain size (d_{DRX}) and the DRX volume fraction (f_{VDRX}) increase as compared with Fig. 1(a). With $\dot{\epsilon}$ increasing to 20 s⁻¹ and 25 s⁻¹, f_{VDRX} further increases, only a small part of un-DRXed region can be observed, and some DRX grains grow up obviously.

Table 1 shows the statistical data of f_{VDRX} and d_{DRX} in the Mg–5Zn–0.6Mn alloy sheets under different $\dot{\epsilon}$. With $\dot{\epsilon}$ rising from 10 to 25 s⁻¹ at 300 °C, d_{DRX} gradually grows from 1.0 to 3.4 μm ; and f_{VDRX} gradually increases from 76 to 93%, indicating that f_{VDRX} and d_{DRX} both increase with the increases of $\dot{\epsilon}$.

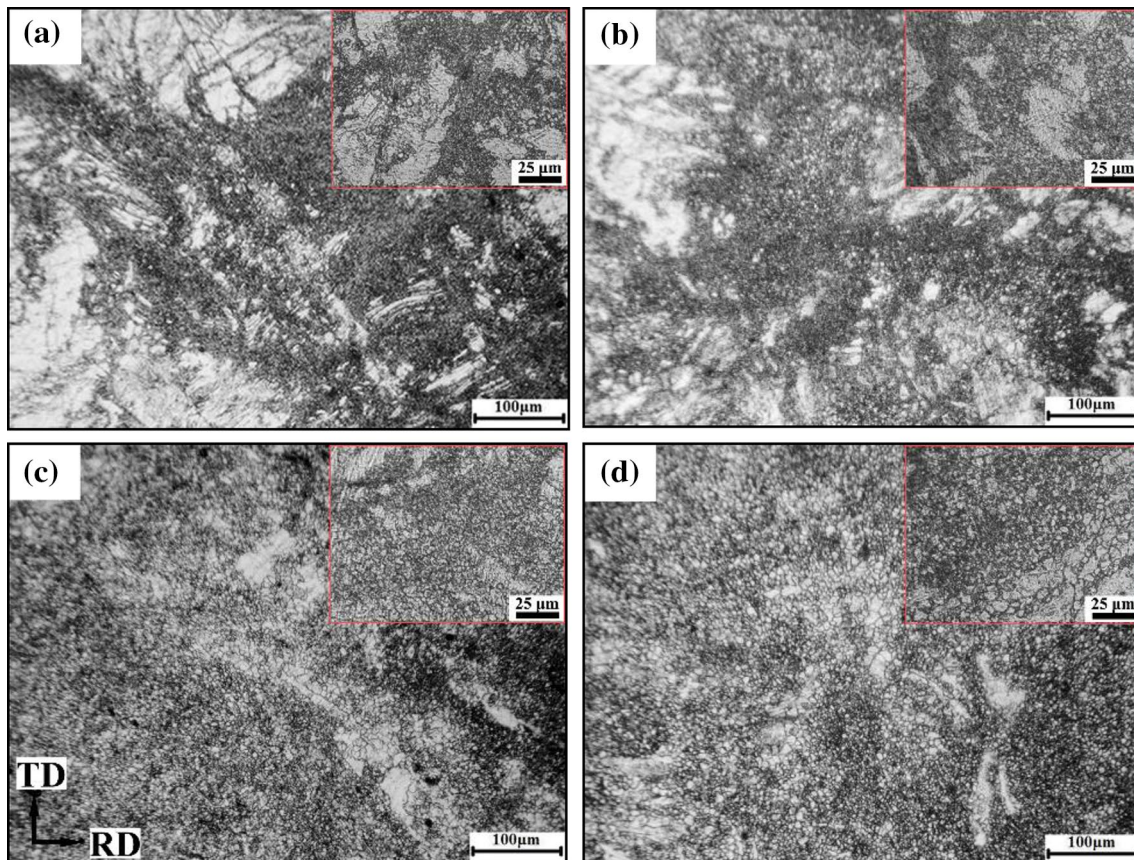


Figure 1: OM images of the alloy sheets rolled at 300 °C with different $\dot{\epsilon}$. (a) 10 s⁻¹; (b) 15 s⁻¹; (c) 20 s⁻¹; (d) 25 s⁻¹.

TABLE 1: DRX grain sizes and volume fractions at different $\dot{\epsilon}$.

Strain rates (s^{-1})	10	15	20	25
d_{DRX} (μm)	1.5 ± 0.3	1.8 ± 0.4	2.5 ± 0.4	3.4 ± 0.6
f_{vDRX} (%)	76 ± 3	81 ± 2	86 ± 1	93 ± 2

Texture evolution

Figure 2 shows the (0002) pole diagrams of the Mg–5Zn–0.6Mn alloy sheets HSRRed at 300 °C with different $\dot{\epsilon}$ (TD–RD direction). Strong basal texture can be observed on all the alloy sheets, that is, the *c*-axis direction of most grains is parallel with the normal direction of the alloy sheets. It can be also found that the distribution characteristics and intensity of basal texture are significantly affected by rolling strain rate.

The maximum intensity value of basal texture is 2.74, and basal texture separates in RD at 10 s^{-1} . When $\dot{\epsilon}$ continues to increase, the maximum intensity value decreases gradually, and the dispersion degree increases. The maximum intensity values of basal texture at 15 s^{-1} , 20 s^{-1} , and 25 s^{-1} are 2.46, 2.21, and 2.09, respectively. Bohlen et al. [15] have also reported that the intensity of (0002) basal component decreases and

the basal plane orientation deflects 10°~20° toward RD in the Mg–Zn–RE alloys. It is reported that the orientation of DRX grains is more random than that of deformed grains, and DRX degree is related to the strength of texture [16, 17]. As shown in Table 1, f_{vDRX} increases with the increases of $\dot{\epsilon}$, resulting in the decrease of basal texture intensity with the increasing $\dot{\epsilon}$.

Mechanical properties

Figure 3 illustrates the room temperature tensile curves of the alloy sheets HSRRed at 300 °C with different $\dot{\epsilon}$. In order to intuitively compare the variation trend of mechanical properties with $\dot{\epsilon}$, the specific values are given in Table 2. It can be seen that the alloy HSRRed at 10 s^{-1} possesses the optimal comprehensive mechanical properties with the tensile strength (UTS) of 321 MPa, yield strength (YS) of 240 MPa, and elongation (EL) of 24.9%. When $\dot{\epsilon}$ increases from 15 to 25 s^{-1} , UTS decreases from 315 to 296 MPa, while EL increases from 25.0 to 27.1%. In general, the increase of $\dot{\epsilon}$ reduces the strength and yield ratio of the alloy sheets, while improving the plasticity, indicating that the secondary forming ability of the sheets will be improved with the increasing $\dot{\epsilon}$.

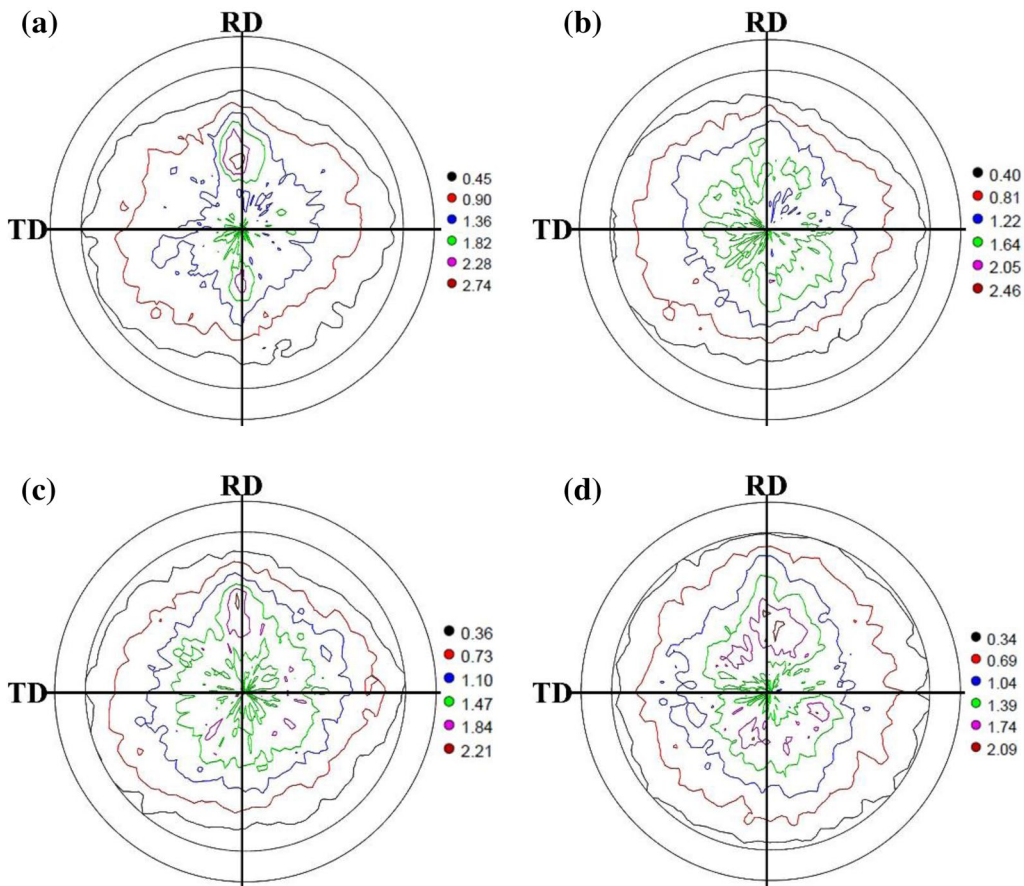


Figure 2: (0002) pole figures of the as-rolled alloy sheets at different $\dot{\epsilon}$. (a) 10 s^{-1} ; (b) 15 s^{-1} ; (c) 20 s^{-1} ; (d) 25 s^{-1} .

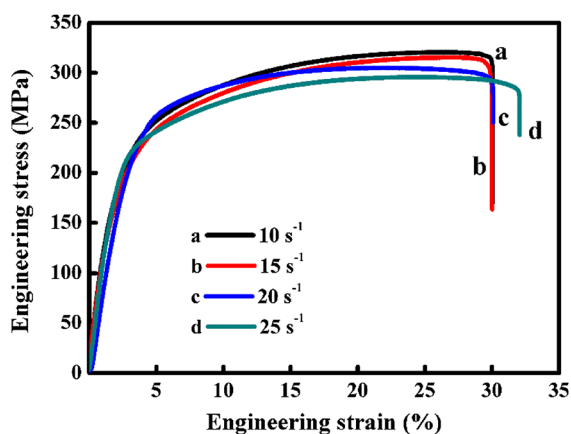


Figure 3: Room temperature tensile properties of the alloy sheets rolled under different $\dot{\epsilon}$.

TABLE 2: Tensile properties of the alloy sheets rolled at 300 °C with different $\dot{\epsilon}$.

Strain rate (s ⁻¹)	UTS (MPa)	YS (MPa)	YS/UTS	EL (%)
10	321 ± 8	240 ± 6	0.75	24.9 ± 0.4
15	315 ± 6	227 ± 4	0.72	25.0 ± 0.2
20	305 ± 3	219 ± 3	0.72	25.2 ± 0.2
25	296 ± 5	206 ± 5	0.70	27.1 ± 0.4

Discussion

Effects of dislocations and twins on texture

During high $\dot{\epsilon}$ deformation, twinning and sliding mechanisms are coordinated and competed with each other, and it also affected by many other factors. Therefore, the relationship between twinning and sliding differs in different conditions, resulting in various texture features [18, 19]. Figure 4(a, b) shows the kernel average misorientation (KAM) maps of the alloy sheets HSRRed at 300 °C with different $\dot{\epsilon}$. KAM map is used to describe the deformation degree of grains and is able to quantitatively calculate geometrically necessary dislocations (GND) [20]. According to the strain gradient theory derived by Kubin et al. [21], the GND density (ρ^{GND}) can be expressed as follows:

$$\rho^{GND} = 2\theta/ub, \quad (1)$$

where θ is the average local misorientation, u represents the electron backscatter diffraction scan step size, and b is Burger's vector (3.21×10^{-10} m [22] for Mg).

The green lines in the KAM maps can be approximately regarded as dislocations. It can be seen from Fig. 4(a) that high-density dislocations and dislocation entanglement can be observed near the original grain boundary and sub-grain boundary at 10 s^{-1} . When $\dot{\epsilon}$ increases to 25 s^{-1} [Fig. 4(b)], many dislocations can still be detected. This is because the work

hardening effect is significant at high $\dot{\epsilon}$, a large number of dislocations are formed, but cannot be fully rearranged and merged as the deformation time is shortened, resulting in dislocation pileup. However, the temperature rise at high $\dot{\epsilon}$ deformation cannot be ignored, as it will reduce the work hardening effect, accelerate the dislocation movement and grain boundary migration, resulting in dislocation consumption and coarsening of DRX grain. Figure 4(c-d) illustrates the distribution of local misorientation at 10 s^{-1} and 25 s^{-1} , the values of ρ^{GND} calculated according to Eq. (1) at 10 s^{-1} and 25 s^{-1} are $5.8 \times 10^{14} \text{ m}^{-2}$ and $4.3 \times 10^{14} \text{ m}^{-2}$, respectively.

In general, twinning is the main coordinated deformation mechanism in the Mg alloys at high $\dot{\epsilon}$ deformation. Twinning can cause a sudden change of grain orientation [23], twin boundaries can also hinder dislocation slip [24], thus affecting the formation and strength of texture. In addition, twinning can also affect DRX, thereby affecting the texture [25]. Figure 4(e, f) shows the twin distribution, the red line represents the tensile twin, the blue line is the compression twin, and the purple line is the double twin. Hong et al. [26] have reported that $\{10\bar{1}2\}$ tensile twins can improve the basal slip activity and modify the basal texture. It can be seen from Fig. 4(e, f) that the red lines representing tensile twins dominate at 10 s^{-1} and 25 s^{-1} , which partly explains the phenomenon that high $\dot{\epsilon}$ deformation can weaken the basal texture.

Effects of DRX on texture

The primary DRX grains with random orientation make a great contribution to the weakening of basal texture, while the DRX grains with a certain orientation grow rapidly at a higher temperature, which greatly increases the texture strength and makes against to texture weaken [27]. Zeng et al. [28] have also found that the recrystallized nuclei with random orientation forms in the early stage are replaced by the selectively grown grains during growth in Mg-0.4Zn alloy, thus forming a strong basal texture. Therefore, DRX behavior has a great influence on texture strength.

Figure 5 illustrates the grain boundary maps, misorientation angle distribution histograms, and grain size distribution diagrams at different $\dot{\epsilon}$. The green lines in Fig. 5(a, b) represent low-angle grain boundaries (LAGBs, misorientation angles of $2^\circ \sim 5^\circ$), the yellow lines are sub-grain boundaries (SGBs, misorientation angles of $5^\circ \sim 15^\circ$), and the black lines are high-angle grain boundaries (HAGBs, misorientation angles higher than 15°). It can be seen that the proportion of HAGBs is smaller at 10 s^{-1} [Fig. 5(a)], while DRX proceeds more adequately as $\dot{\epsilon}$ increases to 25 s^{-1} [Fig. 5(b)]. A peak in the range of $85 \sim 90^\circ$ which represents $\{10\bar{1}2\}$ tensile twin [29] can be observed in both Fig. 5(c and d), and the number of $\{10\bar{1}2\}$ tensile twins increases slightly

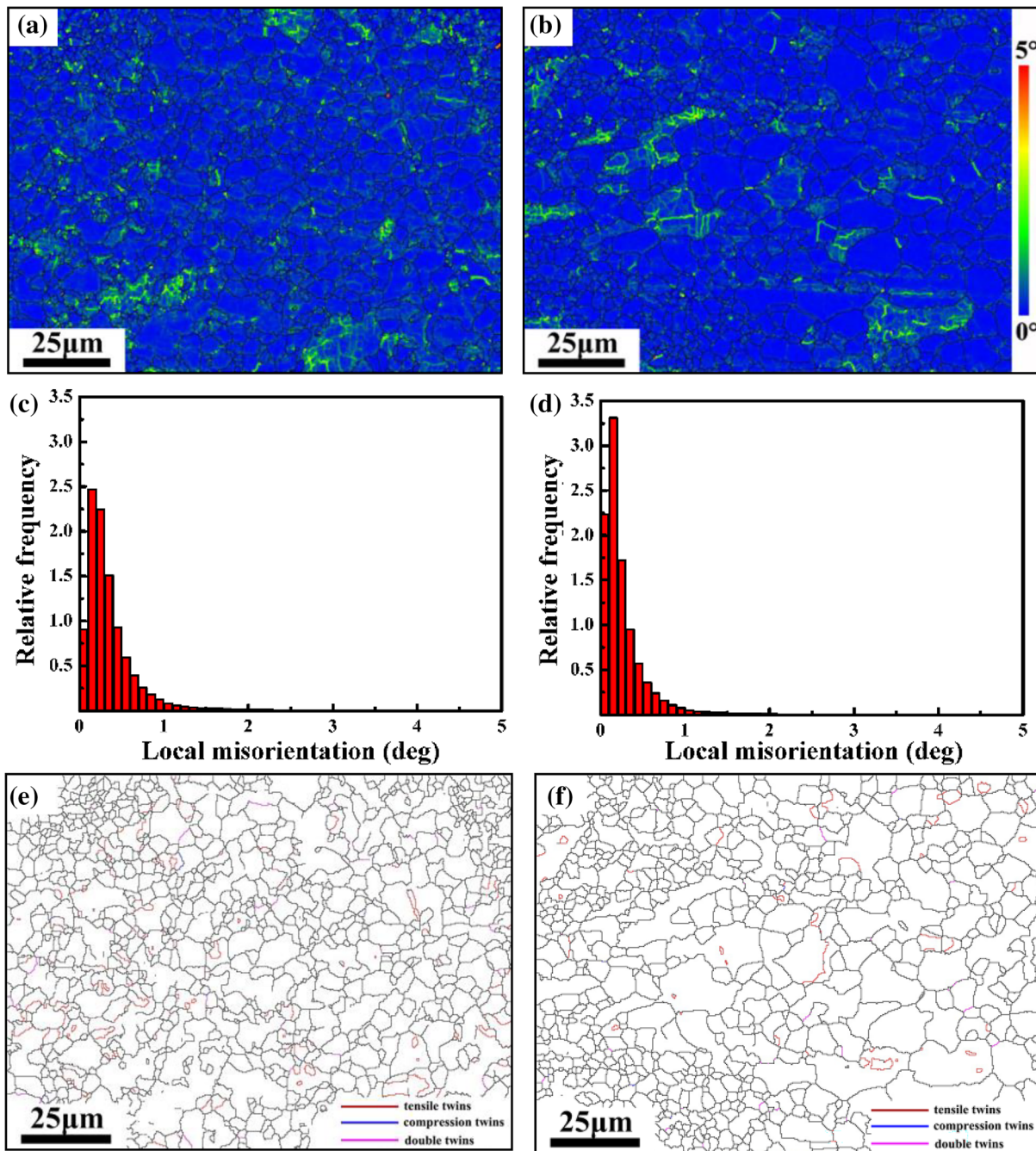


Figure 4: (a–b) KAM maps, (c–d) local misorientation distribution histograms, and (e–f) twins distribution maps of the alloy sheets HSRRed at different $\dot{\epsilon}$, (a, c, and e) 10 s^{-1} ; (b, d, and f) 25 s^{-1} .

with the increase of $\dot{\epsilon}$. In addition, at $\dot{\epsilon}$ of 10 s^{-1} and 25 s^{-1} , the proportion of LAGBs is 6.2% and 6.7%, the proportion of SGBs is 13.9% and 8.2%, respectively. The average grain boundary misorientation (θ_{AV}) and the fraction of HAGBs are 32.4° and 75.6% at 10 s^{-1} , respectively. When $\dot{\epsilon}$ rises to 25 s^{-1} , θ_{AV} and HAGBs fraction values are 40.6° and 81.2% , respectively. As shown in Fig. 5(e), the DRX grain size is mainly concentrated in the range of $1.0 \sim 5.0 \mu\text{m}$ at 10 s^{-1} , the

grains of less than $5.0 \mu\text{m}$ account for about 77.8%, and the average grain size is $3.7 \mu\text{m}$. At 25 s^{-1} [Fig. 5(f)], the average DRX grain size slightly increases to $4.2 \mu\text{m}$ with the grains of less than $5.0 \mu\text{m}$ accounting for about 73.6%. In conclusion, with the increase of $\dot{\epsilon}$ from 10 to 25 s^{-1} , the LAGBs fraction reduces, while the HAGBs fraction, the number of $\{10\bar{1}2\}$ tensile twins, the DRX degree, and average DRX grain size increase.

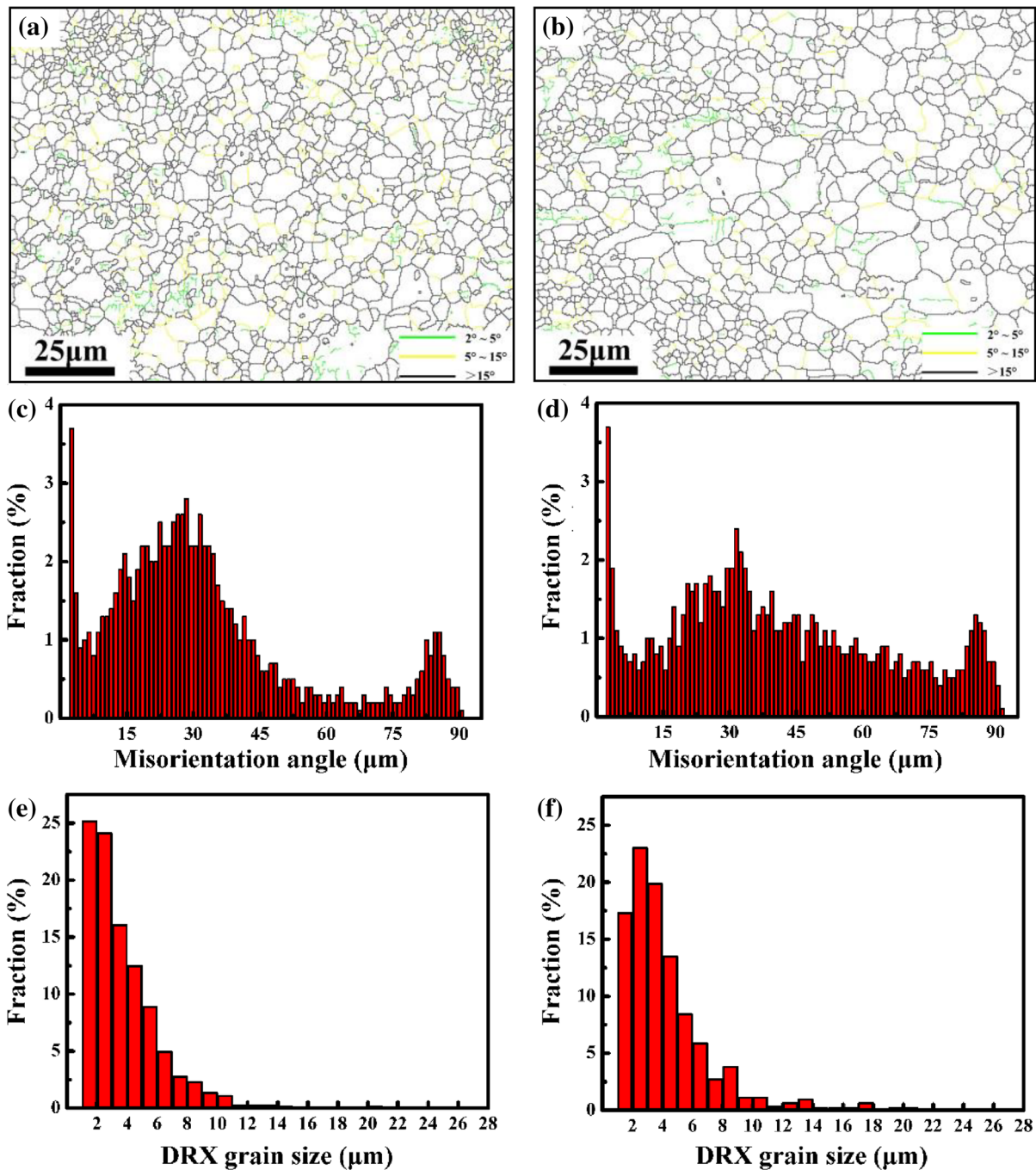


Figure 5: (a–b) Grain boundary maps, (c–d) misorientation angle distribution histograms, and (e–f) grain size distribution diagrams of the alloy sheets HSRRed at different $\dot{\epsilon}$, (a, c, and e) 10 s^{-1} ; (b, d, and f) 25 s^{-1} .

Figure 6 shows the inverse pole figure (IPF) and the pole figure at 10 s^{-1} and 25 s^{-1} . The red color in IPF maps [Fig. 6(a, b)] represents the grain exhibiting (0001) basal plane. It can be seen that both samples exhibit strong (0001) basal texture, and the texture intensity decreases with the increase of $\dot{\epsilon}$. As shown in Fig. 6(c, d), the maximum intensity value of (0001) basal texture at 10 s^{-1} and 25 s^{-1} is 12.64 and 12.08, respectively.

The increase of $\dot{\epsilon}$ accelerates the dislocation multiplication rate, increasing the dislocation density and the driving force of DRX nucleation, resulting in promoting the DRX progress [30]. Twinning is the main plastic deformation mechanism of Mg–Zn alloy during HSRR, and the number of twins increases with the increase of $\dot{\epsilon}$ [31], twins are also conducive to DRX nucleation. Therefore, f_{VDRX} increases with the increasing $\dot{\epsilon}$.

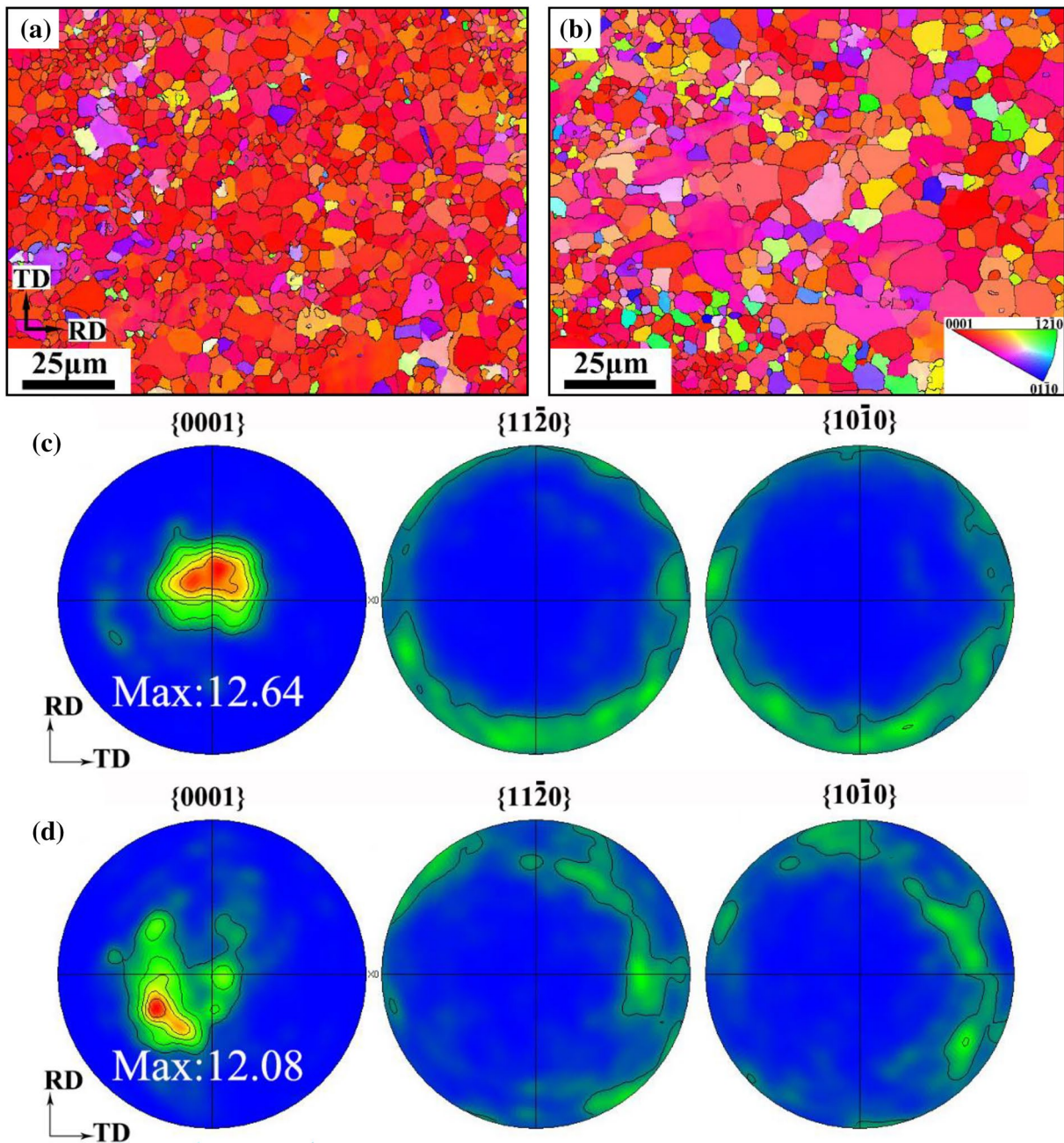


Figure 6: (a–b) IPF maps and (c–d) pole figures of the alloy sheets HSRRed at different $\dot{\epsilon}$, (a) (c) 10 s^{-1} ; (b) (d) 25 s^{-1} .

In addition, the temperature rise during HSRR accelerates the nucleation and grain boundary migration of DRX, resulting in d_{DRX} increasing with the increase of $\dot{\epsilon}$. Previous studies have shown that the orientation of DRX grains is more random than that of the deformed grains [9, 10]. Therefore, when $\dot{\epsilon}$ increases from 10 to 25 s^{-1} , the texture strength decreases with the increase of f_{VDRX} , while the growth of DRX grains is not obvious enough to form a new strong texture, so its contribution to the texture modification is not satisfactory.

Effects of precipitates on texture

The size, spacing, distribution, morphology of the precipitates and the orientation relationship with the matrix are the key factors that affect dislocation movement and grain orientation, and then deformation texture [32, 33]. Wang et al. [34] have also found that the widely distributed Ca-rich phase in Mg–1.0Zn–1.5Ca alloy after hot compression promotes the occurrence of DRX and weakens the texture.

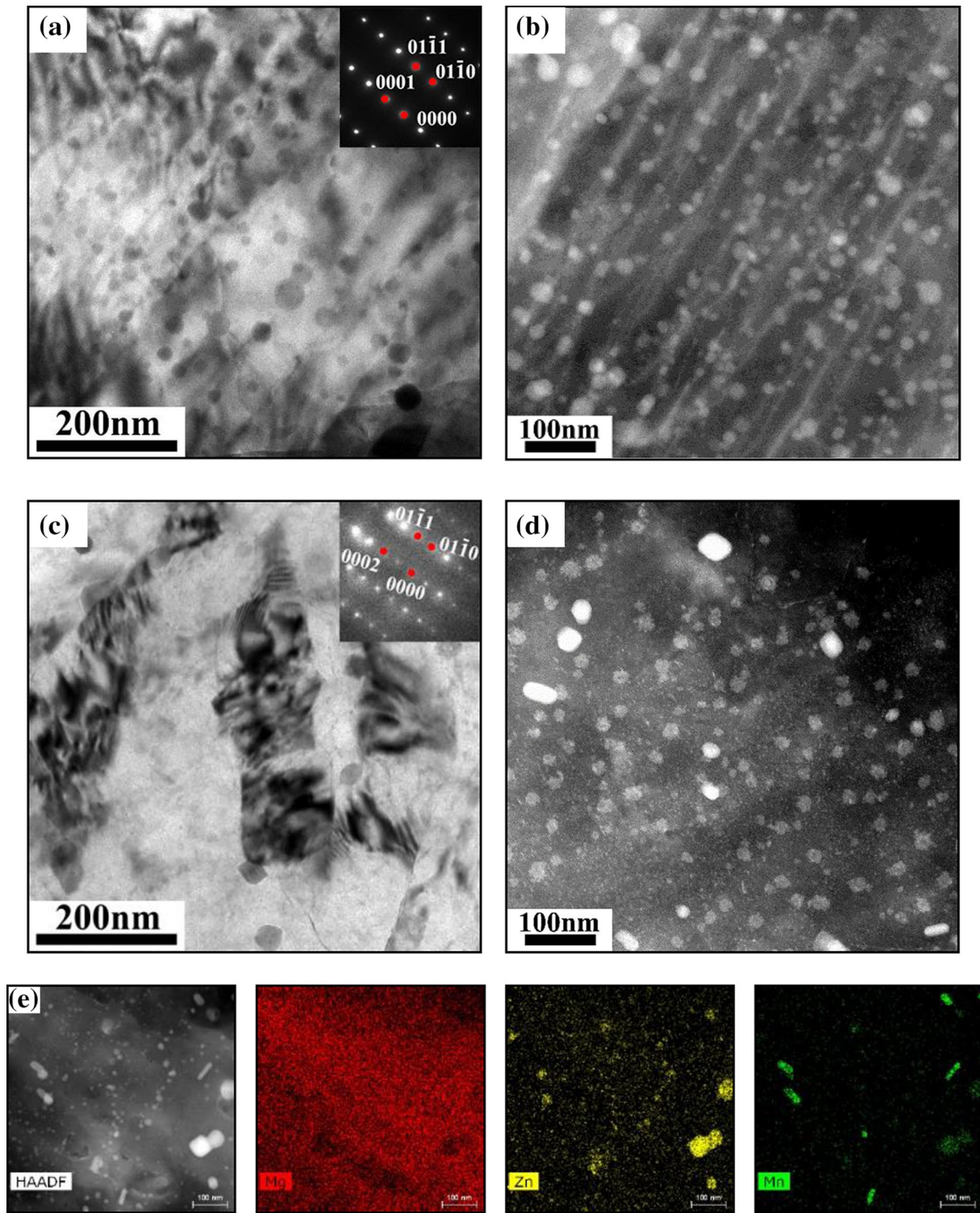


Figure 7: (a), (c) BF-TEM images, (b), (d) STEM images, and (e) the corresponding EDS maps showing the distribution of the alloy sheets HSRRed at different $\dot{\epsilon}$, (a), (b) 10 s^{-1} ; (c), (d) 25 s^{-1} .

Figure 7 illustrates the transmission electron microscopy (TEM) images showing the morphology of precipitates in the alloy sheets HSRRed at different $\dot{\epsilon}$, the electron beam is approximately parallel to $[11\bar{2}0]_{\alpha}$. An enormous number of precipitates

are detected under both samples, and most of them are nearly spherical in shape. The average size of precipitates is $(16 \pm 4) \text{ nm}$ at 10 s^{-1} [Fig. 7(a–b)]; the precipitate density decreases, while the average precipitate size increases slightly to $(19 \pm 4) \text{ nm}$ at

25 s⁻¹ [Fig. 7(c-d)]. The deformation time shortens with increasing $\dot{\epsilon}$, resulting in a shorter precipitation process. In addition, the temperature rise caused by deformation will not only hinder the precipitation, but also lead to the growth of the existing precipitates. Therefore, the precipitate density slightly decreases and the average precipitate size slightly increases with the increase of $\dot{\epsilon}$. These changes in the precipitate characteristics weaken the pinning effect of precipitates on DRX grain rotation. Hence, the texture strength slightly decreases with the joint action of twins, DRX and precipitates. A high-angle annular dark-field scanning transmission electron microscopy (HAADF-STEM) image and the corresponding energy-dispersive spectroscopy (EDS) maps in Fig. 7(e) further describe the composition of the precipitates. It can be seen that the fine near spherical precipitates are Zn-rich phases, and the coarse rod-shaped phases are Mn-rich particles.

Effects of texture on mechanical properties

The main strengthening mechanisms in the wrought Mg alloys are solution strengthening, fine grain strengthening, precipitation strengthening, and work hardening [35]. According to the Hall-Petch formula [36], $\sigma = \sigma_0 + kd^{-1/2}$, where σ represents the strength of polycrystal, σ_0 is the strength of the corresponding single crystal, d is the grain size, and k is a constant, the strength of the Mg alloys is obviously affected by the change of d , due to the K value of the Mg alloys is high up to 280 ~ 320 MPa $\mu\text{m}^{1/2}$ [37]. According to the Orowan mechanism [38], the increases in the precipitation density strengthen the hinder effect of the precipitates on dislocation, thus improving the strength of the alloy. Of course, the more precipitates, the solution strengthening effect will be relevantly weakened. In addition, it can be seen from Fig. 4 that there is still a certain density of dislocations at different $\dot{\epsilon}$, which could bring about work hardening and YS increasing. Therefore, the alloy sheets HSRRed at 10 s⁻¹ possess

the highest strength, due to the smallest d_{DRX} (Table 1), the largest ρ^{GND} (Fig. 4), and precipitation density (Fig. 7).

The influence of texture on the mechanical properties in the Mg alloys is realized by modifying the Schmid factor (SF) of the slip system (particularly basal slip system), which leads to the texture strengthening or weakening [20]. Figure 8 shows SFs of the basal slip system ($\langle a \rangle(0001)[11\bar{2}0]$) with different $\dot{\epsilon}$. SFs ranged mostly from 0.1 to 0.3 at 10 s⁻¹, with the average SF value of 0.24 [Fig. 8(a)], which increases to 0.29 as $\dot{\epsilon}$ increases to 25 s⁻¹ [Fig. 8(b)]. The higher the SF, the better the plastic deformation ability of the alloy. Due to the existence of texture in the alloy, the Schmid factor of grain slip differs in different directions. The slip system with lower critical resolved shear stress and higher SF starts first, resulting in the plasticity increase and the yield strength decrease in this direction, leading to texture softening [39]. Mabuchi et al. [40] have investigated the yield strength of the Mg-9Al-1Zn alloys with same grain size through two different deformation process. It has been found that the conventional hot extrusion samples with higher yield strength of 364 MPa show a texture with the c -axis perpendicular to the extrusion direction, making the basal slip system hard to start. After equal channel angular extrusion, the yield strength of the sample decreases to 277 MPa as its c -axis deviates about 45° with the extrusion direction. The higher SF of the grain basal plane makes it easy to slip, which reduces the deformation resistance and yield strength. This further shows that the texture of the Mg alloy not only affects the mechanical properties, but also has a greater impact on the subsequent secondary formability. Accordingly, the increases of $\dot{\epsilon}$ reduced the yield strength and tensile strength, while improving the plasticity and the secondary processing formability of the Mg-5Zn-0.6Mn alloy sheets, which is consistent with the results in Table 2.

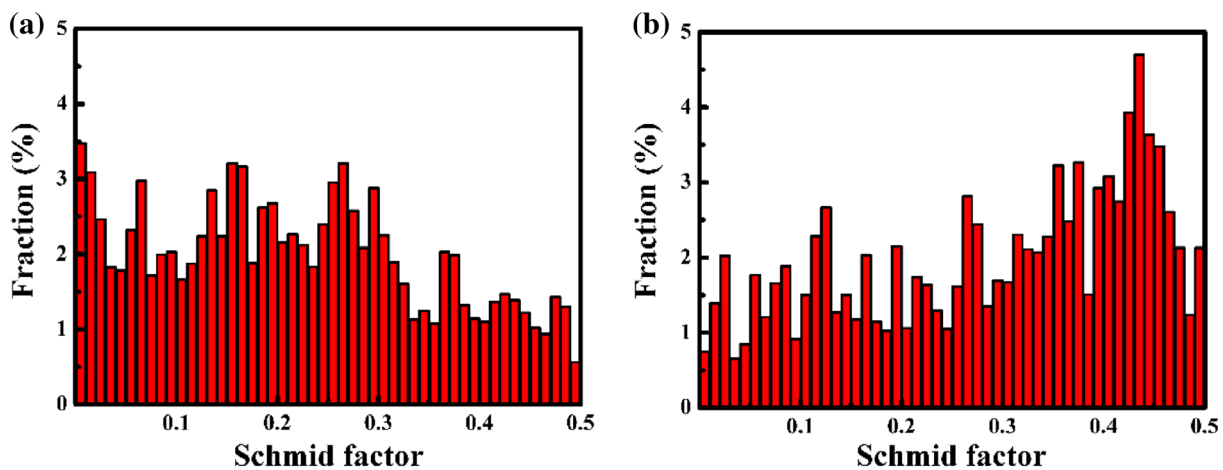


Figure 8: Schmid factors in the alloy sheets HSRRed at different $\dot{\epsilon}$. (a) 10 s⁻¹; (b) 25 s⁻¹.

Conclusion

The effects of strain rates ($\dot{\epsilon}$) on the microstructure, texture, and mechanical properties of the Mg–5Zn–0.6Mn alloy sheets during HSRRed at 300 °C were studied. The effects of dislocation, twinning, DRX and precipitation on texture, and the effect of texture on mechanical properties were also clarified. The conclusions are as follows.

- (1) When the Mg–5Zn–0.6Mn alloy is HSRRed at 10 s⁻¹, 15 s⁻¹, 20 s⁻¹, and 25 s⁻¹, d_{DRX} is 1.0 μm, 1.8 μm, 2.5 μm, and 3.4 μm, and f_{VDRX} is 76%, 81%, 86%, and 93%, respectively. Increasing the rolling strain rate promotes DRX.
- (2) The maximum intensity values of basal texture are 2.74, 2.46, 2.21, and 2.09 at 10 s⁻¹, 15 s⁻¹, 20 s⁻¹, and 25 s⁻¹, respectively. The texture weakens with the increases of $\dot{\epsilon}$, which is mainly attributed to the increase in f_{VDRX} and the number of tensile twins.
- (3) With the increases of $\dot{\epsilon}$, the strength decreases, while the plasticity increases. The alloy sheets HSRRed at 10 s⁻¹ possess the optimal comprehensive mechanical properties with UTS of 321 MPa, YS of 240 MPa and EL of 24.9%, and the highest strength is attributed to the smallest d_{DRX} , the largest ρ^{GND} , and precipitation density.

Experimental details

The Mg–5Zn–0.6Mn (wt%) were prepared by melting pure Mg, pure Zn, Mg–10 wt% Mn master alloy in an electrical resistance furnace followed by casting into a steel mold. The ingots were subjected to a two-step solution treatment (330 °C/24 h + 400 °C/2 h). The as-solutionized alloy plates were machined into 100 mm × 100 mm × 10 mm, and then were rolled in a twin roll mill with the roller size of Φ 360 × 600 mm. The rolling temperature of 300 °C and four rolling strain rates ($\dot{\epsilon}$ = 10 s⁻¹, 15 s⁻¹, 20 s⁻¹, and 25 s⁻¹) were selected in this study. The plates were pre-heated at 300 °C for 15 min before rolling and were rolled with the reduction (λ) of 80% from 10 mm (H) to 2 mm (h) by a single pass. $\dot{\epsilon}$ was calculated by the equation $\dot{\epsilon} = \frac{H-h}{H} \frac{V}{\sqrt{R(H-h)}}$ (see Ref. [41] for detail), where V was the roll circumferential speed (430 mm s⁻¹) and R was the roller radius (180 mm). After rolling, the plates were quenched into water immediately to retain the microstructures.

The as-rolled microstructures were examined on the sections perpendicular to TD and RD. The samples were etched in picric acid solution (0.4 g picric acid + 1 mL acetic acid + 1.5 mL water + 10 mL alcohol) for about 10 s, and then observed on the LeitzMM–6 optical microscope (OM). The average grain size was measured by the intercept methods (ASTM E1382–97, 2015), and Image-Pro Plus 6.0 software

was used to calculate the DRX volume fractions. About 30 fields of view were observed and 8 typical images were acquired for each sample. The DRX volume fraction was calculated in the following manner. First, the total pixel points (A) of an image were obtained by Image-Pro Plus 6.0 software. Second, the pixel points (a) of the deformation area in the image were obtained. Then, the DRX volume fraction V of the alloy was calculated by the following equation, i.e., $V = (A - a)/A$. Finally, the DRX volume fraction of each sample was the average value taken from eight different images (see Ref. [42] for detail). The macro-texture analysis for the as-rolled alloys was performed using X-ray diffraction (XRD; D8 Discover) instrument with CuK α at a scanning rate of 5°/min. The samples for XRD were ground with 2000# waterproof abrasive paper and etched in acetic picral (0.3 g oxalic acid, 1 mL acetic acid, 1.5 mL water, and 10 mL ethanol) for macro-texture measurements. The (0002) pole diagrams of samples were examined on the sections perpendicular to TD and RD, and the TexEval software was used for data analysis. The electron backscatter diffraction (EBSD) analysis was carried out by field emission scanning electron microscopy with a LEO Supra 35 operated at an acceleration voltage of 20 kV and an emission current of 3.0 nA. An Oxford Instruments Nordlys Nano EBSD system equipped with Channel 5 data acquisition and analysis software was used for data collection and analysis. The samples for EBSD measurement were prepared by mechanical polishing and then electropolished in an electrolyte (70% phosphoric acid and 30% distilled water) with a voltage of –12 V and at a temperature of –15 °C for 60 s. The precipitates were observed in a Titan G2 60–300 spherical aberration-corrected transmission electron microscopy. The samples were thinned by the abrasive paper to ~40 μm in thickness, and then were ion thinned on a Gatan precision ion polishing system. In addition, the position of the sample observed by XRD was also used for EBSD and TEM analysis. The mechanical properties were measured on Instron 3369 electronic universal testing machine. The tensile specimens were cut from the as-rolled sheets along RD with 15 mm in gauge length and 4 mm × 2 mm in cross section. Three tensile samples were measured in each strain rate group to ensure the reliability of the data.

Acknowledgments

The authors are grateful to the support of the Scientific Research Fund of Education Department in Hunan Province, China (21C0431 and 21C0408); the National Natural Science Foundation of China Projects (No. 52271177) and the Science and Technology Innovation Leaders Projects in Hunan Province, China (No. 2021RC4036).

Data availability

The raw/processed data required to reproduce these findings cannot be shared at this time as the data also form part of an ongoing study.

Declarations

Conflict of interest The authors declare that they have no conflict of interest.

References

1. L.L. Guo, F. Fujita, Effect of deformation mode, dynamic recrystallization and twinning on rolling texture evolution of AZ31 magnesium alloys. *T. Nonferr. Metal. Soc.* **28**(6), 1094–1102 (2018)
2. M. Masoumi, M. Pegguleryuz, The influence of Sr on the microstructure and texture evolution of rolled Mg–1%Zn alloy. *Mat. Sci. Eng. A* **529**, 207–214 (2011)
3. T. Lasera, M.R. Nürnberg, A. Janz, Ch. Hartig, D. Letzig, R. Schmid-Fetzer, R. Bormann, The influence of manganese on the microstructure and mechanical properties of AZ31 gravity die cast alloys. *Acta Mater.* **54**(11), 3033–3041 (2006)
4. N. Stanford, M.R. Barnett, The origin of “rare earth” texture development in extruded Mg–based alloys and its effect on tensile ductility. *Mater. Sci. Eng. A* **496**(1–2), 399–408 (2008)
5. W.J. Kim, S.J. Yoo, Z.H. Chen, H.T. Jeong, Grain size and texture control of Mg–3Al–1Zn alloy sheet using a combination of equal-channel angular rolling and high-speed-ratio differential speed-rolling processes. *Scr. Mater.* **60**(10), 897–900 (2009)
6. S.W. Pan, Y.C. Xin, G.J. Huang, Q. Li, F.L. Guo, Q. Liu, Tailoring the texture and mechanical anisotropy of a Mg–2Zn–2Gd plate by varying the rolling path. *Mater. Sci. Eng. A* **653**, 93–98 (2016)
7. H.M. Chen, H.S. Yu, S.B. Kang, G.H. Min, Y.X. Jin, Effect of rolling temperature on microstructure and texture of twin roll cast ZK60 magnesium alloy. *Trans. Nonferr. Metal. Soc.* **20**(11), 2086–2091 (2010)
8. M. Sanjari, A.S.H. Kabir, A. Farzadfar, H. Utsunomiya, R. Petrov, L. Kestens, S. Yue, Promotion of texture weakening in magnesium by alloying and thermomechanical processing. II: rolling speed. *J. Mater. Sci.* **49**(3), 1426–1436 (2013)
9. J.X. Liu, K. Liu, W.B. Du, S.B. Li, Z.H. Wang, X. Du, C.C. Sun, Effect of temperature on microstructure and texture evolution of Mg–Zn–Er alloy during hot compression. *Trans. Nonferr. Metal. Soc.* **28**(11), 2214–2225 (2018)
10. M.Y. Zheng, L.B. Tong, S.W. Xu, X.S. Hu, K. Wu, S. Kamado, Microstructure and mechanical properties of extruded Mg–Zn–Ca alloy. *Mater. Sci. Forum* **654**, 703–706 (2010)
11. H.N. Liu, Y.J. Li, Z. Kui, X.G. Li, K.K. Wang, Microstructure, hot deformation behavior, and textural evolution of Mg–3wt%Zn–1wt%Ca–0.5wt%Sr alloy. *J. Mater. Sci.* **55**(32), 12434–12447 (2020)
12. S.Q. Zhu, H.G. Yan, J.H. Chen, Y.Z. Wu, Y.G. Du, X.Z. Liao, Fabrication of Mg–Al–Zn–Mn alloy sheets with homogeneous fine-grained structures using high strain-rate rolling in a wide temperature range. *Mater. Sci. Eng. A* **559**, 765–772 (2013)
13. S.Q. Zhu, H.G. Yan, X.Z. Liao, S.J. Moody, G. Sha, Y.Z. Wu, S.P. Ringer, Mechanisms for enhanced plasticity in magnesium alloys. *Acta Mater.* **82**, 344–355 (2015)
14. S.W. Xu, S. Kamado, N. Matsumoto, T. Honma, Y. Kojima, Recrystallization mechanism of as-cast AZ91 magnesium alloy during hot compressive deformation. *Mater. Sci. Eng. A* **527**, 52–60 (2009)
15. J. Bohlen, M.R. Nürnberg, J.W. Senn, D. Letzig, S.R. Agnew, The texture and anisotropy of magnesium–zinc–rare earth alloy sheets. *Acta Mater.* **55**(6), 2101–2112 (2007)
16. I. Basu, T. Al-Samman, Triggering rare earth texture modification in magnesium alloys by addition of zinc and zirconium. *Acta Mater.* **67**, 116–133 (2014)
17. S.A. Farzadfar, É. Martin, M. Sanjari, E. Essadiqi, S. Yue, Texture weakening and static recrystallization in rolled Mg–2.9Y and Mg–2.9Zn solid solution alloys. *J. Mater. Sci.* **47**(14), 5488–5500 (2012)
18. É. Martin, R.K. Mishra, J.J. Jonas, Effect of twinning on recrystallisation textures in deformed magnesium alloy AZ31. *Philos. Mag.* **91**(27), 3613–3626 (2011)
19. H. Somekawa, Y. Osawa, A. Singh, K. Washio, T. Mukai, Effect of micro-alloying elements on deformation behavior in Mg–Y binary alloys. *Mater. Trans.* **55**(1), 182–187 (2014)
20. X.L. Ma, C.X. Huang, J. Moering, M. Ruppert, H.W. Höppel, M. Göken, J. Narayan, Y.T. Zhu, Mechanical properties of copper/bronze laminates: role of interfaces. *Acta Mater.* **116**, 43–52 (2016)
21. L.P. Kubin, A. Mortensen, Geometrically necessary dislocations and strain-gradient plasticity: a few critical issues. *Scr. Mater.* **48**(2), 119–125 (2003)
22. E. Nes, B. Holmedal, E. Evangelista, K. Marthinsen, Modelling grain boundary strengthening in ultra-fine grained aluminum alloys. *Mater. Sci. Eng. A* **410–411**, 178–182 (2005)
23. X. Zhao, K. Zhang, X.G. Li, Y.J. Li, Q.B. He, J.F. Sun, Deformation behavior and dynamic recrystallization of Mg–Y–Nd–Gd–Zr alloy. *J. Rare Earths* **26**(6), 846–850 (2008)
24. A. Chapuis, B. Wang, Q. Liu, A comparative study between uniaxial compression and plane strain compression of Mg–3Al–1Zn alloy using experiments and simulations. *Mater. Sci. Eng. A* **597**, 349–358 (2014)
25. P. Yang, L. Meng, X. Li, W. Mao, L. Chen, *Microstructure and micro-texture evolution of compression twins in magnesium* (Wiley, New York, 2008), pp.159–163
26. S.G. Hong, S.H. Park, C.S. Lee, Role of 10–12 twinning characteristics in the deformation behavior of a polycrystalline magnesium alloy. *Acta Mater.* **58**(18), 5873–5885 (2010)

27. Z.H. Chen, W.J. Xia, Y.Q. Chen, D.F. Fu, Texture and anisotropy in magnesium alloys. *Chin. J. Nonferr. Metal.* **15**(1), 1–11 (2005)
28. Z.R. Zeng, Y.M. Zhu, S.W. Xu, M.Z. Bian, J.F. Nie, Texture evolution during static recrystallization of cold-rolled magnesium alloys. *Acta Mater.* **105**, 479–494 (2016)
29. M.G. Jiang, C. Xu, H. Yan, G.H. Fan, T. Nakata, C.S. Lao, R.S. Chen, S. Kamado, E.H. Han, B.H. Lu, Unveiling the formation of basal texture variations based on twinning and dynamic recrystallization in AZ31 magnesium alloy during extrusion. *Acta Mater.* **157**, 53–71 (2018)
30. L.Q. Shen, Q. Yang, L. Jin, J. Dong, Deformation behavior and microstructure transformation of AZ31B Mg alloy under high strain rate compression. *Chin. J. Nonferr. Metal.* **24**(9), 2195–2204 (2014)
31. B.H. Lee, W. Bang, S. Ahn, C.S. Lee, Effects of temperature and strain rate on the high-temperature workability of strip-cast Mg–3Al–1Zn alloy. *Metall. Mater. Trans A* **39**(6), 1426–1434 (2008)
32. H.T. Jiang, Z. Ma, Z.X. Cai, Y. Shu, Q. Kang, Texture and room-temperature formability of rolled Mg–1.5Zn–xCe alloys. *Chin. J. Eng.* **37**(2), 204–210 (2015)
33. Q.F. Wang, W.B. Du, K. Liu, Z.H. Wang, S.B. Li, K. Wen, Microstructure, texture and mechanical properties of as-extruded Mg–Zn–Er alloys. *Mater. Sci. Eng. A* **581**, 31–38 (2013)
34. H.L. Ding, T.Y. Wang, C.Z. Xu, D.K. Li, Effects of Ca addition and deformation conditions on microstructure and texture of Mg–Zn alloy. *Chin. J. Nonferr. Metal.* **25**(5), 1142–1152 (2015)
35. S.M. He, X.Q. Zeng, L.M. Peng, X. Gao, J.F. Nie, W.J. Ding, Microstructure and strengthening mechanism of high strength Mg–10Gd–2Y–0.5Zr alloy. *J. Alloys Compd.* **427**(1–2), 316–323 (2007)
36. W. Sylwestrowicz, E.O. Hall, The deformation and ageing of mild steel. *Proc. Phys. Soc. B* **64**(6), 495–502 (1951)
37. B.Q. Han, D.C. Dunand, Microstructure and mechanical properties of magnesium containing high volume fractions of yttria dispersoids. *Mater. Sci. Eng. A* **277**(1–2), 297–304 (2000)
38. J.F. Nie, Effects of precipitate shape and orientation on dispersion strengthening in magnesium alloys. *Scr. Mater.* **48**(8), 1009–1015 (2003)
39. W.N. Tang, R.S. Chen, J. Zhou, E.H. Han, Effects of ECAE temperature and billet orientation on the microstructure, texture evolution and mechanical properties of a Mg–Zn–Y–Zr alloy. *Mater. Sci. Eng. A* **499**(1–2), 404–410 (2009)
40. M. Mabuchi, Y. Chino, H. Iwasaki et al., The grain size and texture dependence of tensile properties in extruded Mg–9Al–1Zn. *Mater. Trans.* **42**(7), 1182–1188 (2001)
41. S.Q. Zhu, H.G. Yan, J.H. Chen, Y.Z. Wu, B. Su, Y.G. Du, X.Z. Liao, Feasibility of high strain-rate rolling of a magnesium alloy across a wide temperature range. *Scr. Mater.* **67**, 404–407 (2012)
42. H.G. Yan, Q. Wu, J.H. Chen, W.J. Xia, M. Song, B. Su, J. Wu, Microstructure evolution and mechanical properties of the ZM61 alloy sheets under different pre-rolling and high strain rate rolling temperatures. *J. Mater. Res.* **35**(14), 1817–1824 (2020)

Publisher's Note Springer Nature remains neutral with regard to jurisdictional claims in published maps and institutional affiliations.

Springer Nature or its licensor (e.g. a society or other partner) holds exclusive rights to this article under a publishing agreement with the author(s) or other rightsholder(s); author self-archiving of the accepted manuscript version of this article is solely governed by the terms of such publishing agreement and applicable law.